Journal of Materials Science & Technology 181 (2024) 231–239

Contents lists available at ScienceDirect

Journal of Materials Science & Technology

journal homepage: www.elsevier.com/locate/jmst

Research Article

Plasticity and rejuvenation of aged metallic glasses by ultrasonic vibrations

Zhe Chen[a], Shuai Ren[a,b,*], Rui Zhao[c], Jian Zhu[a], Xin Li[d], Heting Zhang[a], Hongji Lin[a], Jiahua Zhu[a], Sajad Sohrabi[a], Wenqing Ruan[a,*], Jiang Ma[a,b,*]

[a] *Guangdong Key Laboratory of Electromagnetic Control and Intelligent Robots, Shenzhen University, Shenzhen 518060, China*
[b] *Shenzhen Key Laboratory of High Performance Nontraditional Manufacturing, College of Mechatronics and Control Engineering, Shenzhen University, Shenzhen 518060, China*
[c] *Institute of Physics, Chinese Academy of Sciences, Beijing 100190, China*
[d] *School of Mechanical, Electrical and Information Engineering, Shandong University, Weihai 264209, China*

ARTICLE INFO

Article history:
Received 27 June 2023
Revised 22 August 2023
Accepted 16 September 2023
Available online 9 November 2023

Keywords:
Metallic glass
Ultrasonic vibration induced plasticity
Aging
Rejuvenation

ABSTRACT

Metallic glasses (MGs) possess exceptional properties, but their properties consistently deteriorate over time, thereby resulting in increased complexity in processing. It thus poses a formidable challenge to the forming of long-term aged MGs. Here, we report ultrasonic vibration (UV) loading can lead to large plasticity and strong rejuvenation in significantly aged MGs within 1 s. A large UV-induced plasticity (UVIP) of 80% height reduction can be achieved in LaNiAl MG samples aged at 85% of its glass transition temperature ($0.85T_g$) for a duration of up to 1 month. The energy threshold required for UVIP monotonously increases with aging time. After the UV loading process, the aged samples show strong rejuvenation, with the relaxation enthalpy even surpassing that of as-cast samples. These findings suggest that UV loading is an effective technique for forming and rejuvenating aged MGs simultaneously, providing an alternative avenue to explore the interplay between the property and microstructures as well as expanding the application prospects of MGs.

1. Introduction

Metallic glasses (MGs) are unique materials that are synthesized by quenching molten liquids at relatively high cooling rates to prevent crystallization [1–5]. Their unique characteristics stem from the absence of long-range ordering and conventional defects like dislocations and grain boundaries. As a result, MGs exhibit many desirable properties, including large elastic limits, high strength, high wear resistance, and high corrosion resistance [6–11]. However, as a kind of metastable material, MGs tend to present a transition toward a more stable low-energy state under applied stress, high-temperature, or even natural conditions, known as aging or structural relaxation, resulting in a deterioration in properties.

For instance, thermoplastic forming is a commonly employed technique for shaping MGs [12–15], which has successfully produced bulk MGs on a large scale [16]. However, the thermoplastic forming process involves heating MGs to their supercooled liquid region [17], which unavoidably results in property degradation. Consequently, the MGs after thermoplastic forming necessitate subsequent treatments to restore their properties, highlighting the significance of rejuvenation in MGs. Thus, the rejuvenation of MGs has been an important issue in MGs [18–39]. In recent years, numerous approaches have been employed to rejuvenate metallic glass. These methods either are closely associated with elastic deformation like elastostatic deformation [18,19], thermal cycling [20,21], and high-pressure annealing [22,23], or are tightly related to plastic deformation, such as triaxial compression [24], cold rolling [25–28], and high-pressure torsion (HPT) [29–32]. However, these techniques are generally time-consuming and costly, making their application in manufacturing processes challenging. Consequently, there is a pressing need to develop a convenient one-step processing approach that incorporates structural rejuvenation.

On the other hand, property degradation in MGs is also inevitable over time under natural conditions, namely the aging effect, which is most notably seen in an increase in brittleness [40,41]. This aging effect significantly limits the potential applications of MGs and poses challenges in their processing and manufacturing [40,42]. Therefore, it is of importance to explore

---

[*] Corresponding authors at: Guangdong Key Laboratory of Electromagnetic Control and Intelligent Robots, Shenzhen University, Shenzhen 518060, China.

E-mail addresses: shuai.ren@szu.edu.cn (S. Ren), ruanwq@szu.edu.cn (W. Ruan), majiang@szu.edu.cn (J. Ma).

https://doi.org/10.1016/j.jmst.2023.09.029
1005-0302/© 2023 Published by Elsevier Ltd on behalf of The editorial office of Journal of Materials Science & Technology.

innovative approaches to facilitate the processing and forming of aged MGs.

Recently, it has been found that ultrasonic vibration (UV) loading can effectively soften MGs, leading to a pronounced UV-induced plasticity (UVIP) [43–45]. The softening effect of UV on MGs enables the processing and fabrication of amorphous alloys at room temperature [43,44]. The mechanism responsible for the softening effect is related to the excitation of flow units (or soft zones) induced by UV loading, which is primarily linked to the localized β-relaxation process in MGs. Many studies have demonstrated that β-relaxation plays a central role in various properties of MGs, including the mechanical behaviors and the aging effect [46–50]. It has been reported that there are reversible and irreversible β-relaxations in MGs, while a long-time aging process may strongly decrease both of them [51]. Consequently, it invites an interesting question of whether or not UV loading can cause the softening effect in the long-term aged MGs, which holds considerable significance not only in the processing and forming of MGs but also in the adjustment of their energy states and properties.

In this study, we report that UV loading can make the long-term aged MGs soften and strongly rejuvenate within short time scales. Despite that cylindrical samples are aged at 85% of their glass transition temperature (0.85T_g) for a duration of up to 672 h (about 1 month), an excellent UV-induced plasticity of 80% height reduction is still achieved within 1 s. The energy threshold required to achieve softening increases as the aging time increases. Strong rejuvenation after UV loading is determined, which is explained through a schematic energy landscape. Complex-shaped structures of MGs are formed using ultrasonic vibration loading. Our work provides a feasible method to form and rejuvenate the aged MGs simultaneously.

2. Methods

In this work, the $La_{60}Ni_{15}Al_{25}$ (at.%) alloy (abbreviated as La60 hereafter) was synthesized by arc melting pure La (99.9 at.%), Ni (99.999 at.%), and Al (99.999 at.%) in a high purity argon atmosphere. The melting process was carried out using titanium getters at high temperatures to avoid oxidation. To ensure a homogeneous composition of the molten alloy, each ingot was melted 8–10 times, then the ingots were cast into cylindrical rods with a diameter of 2 mm by means of a water-cooled copper mold and cut into small cylinders with a height of 2.5 mm by using a low-speed diamond saw. The aged samples were obtained by annealing them at different times in a tubular annealing furnace with the protective atmosphere of argon gas.

The phase structure of the samples was examined using X-ray diffraction of Cu K_α radiation (XRD, Rigaku MiniFlex 600). The thermal properties of the samples were determined using differential scanning calorimetry (DSC, Perkin Elmer DSC-8000) at a heating rate of 20 K min^{-1}. The micromorphology and elemental distribution of the samples were characterized using transmission electron microscopy (TEM, FEI F30) and energy-dispersive X-ray spectroscopy (EDS). The TEM samples were prepared on a FEI Scios SEM/FIB dual beam system. The relaxation features were analyzed by a dynamic mechanical analyzer (DMA, TA Q850). The morphology of DMA samples is 20 mm × 1.5 mm × 2 mm. A single cantilever mode was employed.

The vibration loading was done by a homemade ultrasonic device equipped with force and temperature detection attachments that can vibrate at 20 kHz with an amplitude of up to 40 µm. During the ultrasonic treatment, the sample was placed on a mold with a limiting slot of 2.05 mm in diameter and 0.3 mm in depth. A high-speed camera with a frame rate of 4000 fps was used to capture images of the UV process.

3. Results and discussion

3.1. Property changes of samples annealed at 0.85T_g over time

Fig. 1(a) shows the DSC curves of the La60 sample annealed at 0.85T_g (388 K). A broad exothermic peak below T_g is found in the DSC curve of the as-cast sample, corresponding to an irreversible structural relaxation with the annihilation of excess free volume or other structural defects [51–54]. As the annealing time increases, this broad exothermic peak gradually disappears, while an endothermic sub-T_g peak takes place and shifts to the higher temperature. The sub-T_g signal finally merges with the glass transition and an overshoot above T_g appears when the annealing time is longer than 168 h. These results are consistent with previous work [51].

To separate the enthalpy contribution of the irreversible structural relaxation and the sub-T_g peak, we employed the method used in the reference [51]. A standard sample was obtained through the following annealing treatment: heating the sample to T_g + 30 K at a rate of 10 K min^{-1}, annealing it at this temperature for 0.5 min, and subsequently cooling it down at a rate of 100 K min^{-1}, this curve is taken as a reference, as shown by the black curve in the inset of Fig. 1(b). Subsequently, the enthalpy corresponding to the irreversible structural relaxation (blue area) and the sub-T_g peak (red area) can be calculated. Fig. 1(b) exhibits the enthalpy change of the structural relaxation and sub-T_g peak with annealing time. It is noted that the enthalpy of the structural relaxation gradually decreases, while that of the sub-T_g peak gradually enhances. According to the reference [51], the enthalpy of the structural relaxation corresponds to the annihilation of the irreversible β-relaxation, while that of the sub-T_g peak stems from the required activation energy to excite the reversible β-relaxation. As a result, these results in Fig. 1(b) indicate the 0.85T_g-annealed samples become more and more stable as the annealing time increases.

To further quantify the thermodynamic stability of aged metallic glasses, we measured the fictive temperature T_f which is defined as the temperature of equilibrium during the sudden return to the glassy state from a certain state [55–57]. T_f is typically considered to be approximately equal to the T_g from the cooling process [57]. It is obtained from the intersection between the extrapolated glass and liquid lines. Fig. 1(c) shows that ΔT_f (the difference between T_f in the as-cast curve and that in the post-aging curve) steadily increases with the increase in aging time, demonstrating the thermodynamic stability of the aged metallic glass enhanced over aging time.

The XRD spectra in Fig. 1(d) after annealing all maintain halo peaks the same as those of as-cast samples, indicating that the aged samples remain an amorphous structure at the average structure. The high-resolution transmission electron microscopy (HRTEM) image and the corresponding selected area electron diffraction pattern (SAED) of the sample aged at 0.85T_g for 168 h are shown in Fig. 1(e). No visible crystalline phase is found, implying that the annealed sample is fully amorphous at the atomic level.

In Fig. 2(a), the mechanical relaxation spectra of as-cast and aged MGs measured at 1 Hz by DMA are compared. The peak temperature of the β-relaxation increases and the peak intensity decreases with an increase in the aging time. A much clearer view of the peak temperature change can be found in the inset of Fig. 2(a). We then calculated the activation energy barriers of β-relaxation for different aging times according to the Arrhenius formula. Fig. 2(b) shows the relation of frequency and peak temperature for different aging times. The line is obtained from the Arrhenius fitting $f = f_0 \times \exp(-E_a/RT_\beta)$, where f_0 is the prefactor, E_a is the activation energy barrier of the β-relaxation, R is the gas constant, and T_β is the peak temperature of β-relaxation

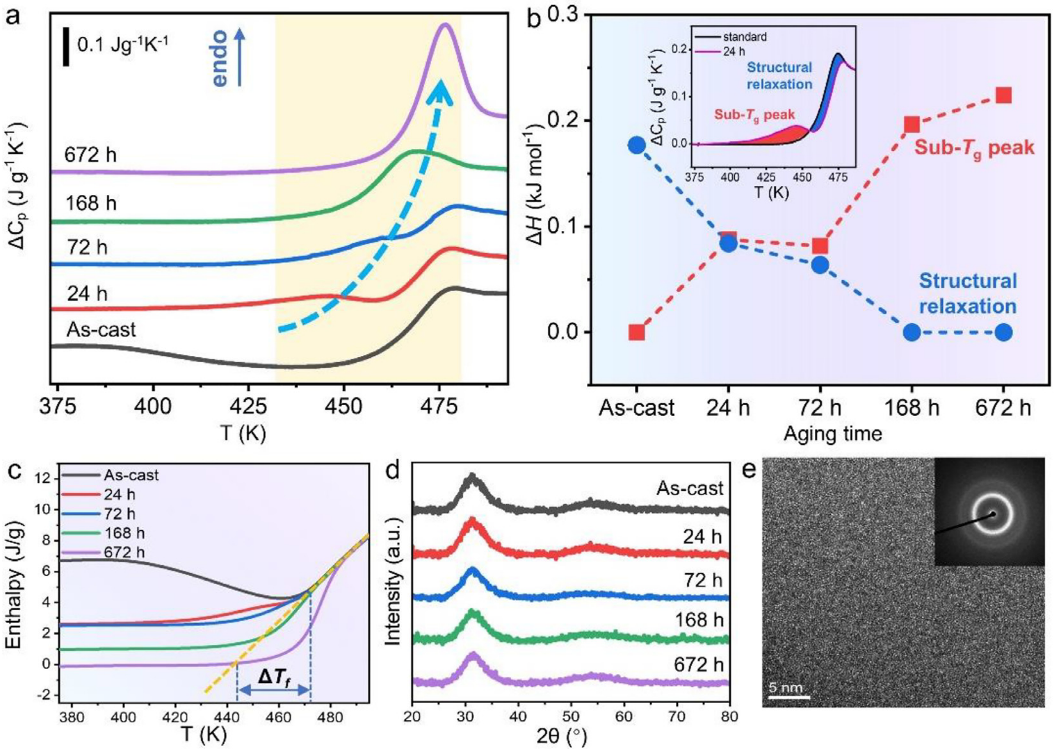

Fig. 1. Property changes of La60 MGs aged at 0.85 T_g. (a) DSC plots of alloys aged at 0.85 T_g for different times. The cyan arrow shows that the sub-T_g peaks enhance and shift towards higher temperatures as the aging time increases. (b) Enthalpy values of sub-T_g peak (red curve) and structural relaxation process (blue curve) of aged MGs. The inset shows the determination method of the enthalpy value of the sub-T_g peak (red area) and structural relaxation process (blue area). (c) Enthalpy curves by integrating the heat capacity shown in (a). (d) XRD curves at different aging times. (e) HRTEM images and corresponding SAED images of the sample aging at 0.85T_g for 168 h.

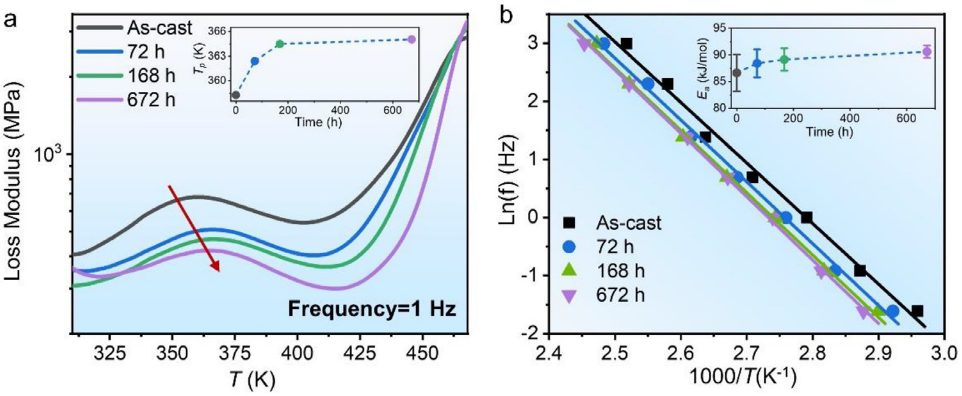

Fig. 2. Dynamic characteristics of aged MGs at different aging temperatures. (a) Loss moduli at 1 Hz for different aging time. The inset shows the peak temperature of β-relaxations as a function of aging time. (b) Arrhenius fitting of β-relaxation of the aged metallic glass. The inset shows the activation energy barrier change with aging time.

[49,58,59]. The value of E_a is then yielded accordingly, which is shown in the inset of Fig. 2(b). It increases steadily with the increase in aging time, with values of 86.638 ± 3.433 kJ mol^{-1} for as-cast, 88.427 ± 2.626 kJ mol^{-1} for 72 h annealing, 89.148 ± 2.115 kJ mol^{-1} for 168 h, and 90.618 ± 1.155 kJ mol^{-1} for 672 h. The increase of peak temperature as well as the activation energy barriers also demonstrate that the longer the annealing time is, the more stable the aged sample is.

3.2. Behavior of aged samples under ultrasonic vibration loading

It is widely recognized that MGs with aging for an extended period of time have a marked increase in brittleness, which significantly impacts their production and utilization of them. Thus, it is of utmost importance to overcome this shortcoming for the processing of aged MGs. On the other hand, as-cast MGs have been found to exhibit ultrasonic vibration-induced plasticity, namely the UVIP. Therefore, it is interesting to explore whether the aged MGs can also exhibit the UVIP.

A schematic diagram of UV loading is shown in Fig. 3(a), which illustrates the basic structure of ultrasonics as well as the state and position of the sample. The ultrasonic horn moves downward at a uniform rate, contacts the sample, and imposes a compressive force on the sample. We choose a stress of 7 MPa as the trigger condition for ultrasonic release. Fig. 3(b–d) presents the stress change during UV loading with ultrasonic vibration release energy of 30 J in the as-cast sample and release energies of 30 and 45 J in the 168-h heat-treated sample, respectively. It is evident that the loading stress is generally low (< 65 Mpa) and the response time is as short as 0.5 s. The abrupt stress drops in Fig. 3(b, d) originate

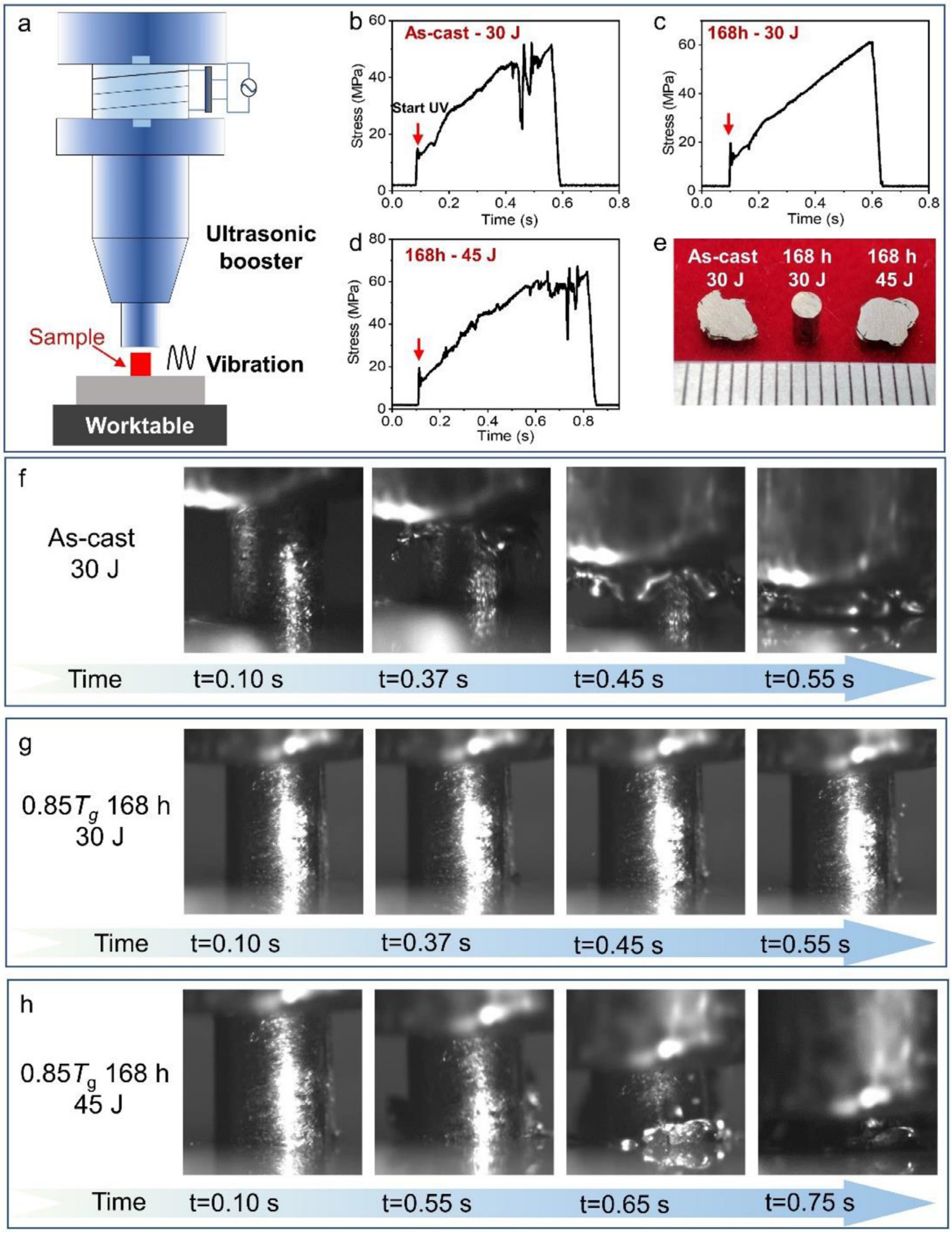

Fig. 3. Behaviors of metallic glasses under UV loading for different aging times. (a) Schematic diagram of the ultrasonic equipment. (b–d) Stress versus time during UV loading, including (b) 30 J applied to As-cast MG, (c) 30 J applied to MG aged at 0.85 T_g for 168 h, and (d) 45 J applied to MG aged at 0.85 T_g for 168 h. (e) Sample pictures of MGs after ultrasonic loading. (f–h) Pictures taken by the high-speed camera during ultrasonic loading.

from the deformation of the sample, which can be clearly seen in Fig. 3(e). As shown in Fig. 3(e), the original sample is softened and eventually compressed into a thin disk under the ultrasonic energy of 30 J, exhibiting a height reduction of ~80%. In comparison, the 168-h aged sample is not deformed under the energy of 30 J, but it is deformed into a thin disk with a reduction of ~80% as the release energy increases to 45 J. Fig. 3(f–h) shows the sample pictures taken by a high-speed camera during the ultrasonic vibration loading process (also refer to Supplementary Videos S1–S3). The as-cast sample in Fig. 3(f) exhibits an obvious fluid-like behavior under a release energy of 30 J. In contrast, the 168-h aged sample shows no plastic deformation under the energy of 30 J in Fig. 3(g). When the released energy increases to 45 J, the 168-h aged sample exhibits a fluid-like behavior, as shown in Fig. 3(h). This finding suggests that the long-term aged sample can still exhibit a large extent of plasticity under UV loading, but larger ultrasonic energies are required to activate plasticity compared to that for the as-cast sample.

To further quantify this phenomenon, we conducted a systematic study to determine the critical energy values required for the softening at different annealing times. UV loading tests were performed on ten samples at different aging times and release energies, as shown in Fig. 4(a). It is evident that, at a given ultrasonic energy, the sample number of deformation decreases with increasing aging time. In addition, at a given aging time, the sample number of deformation keeps increasing with the increase of ultrasonic energy.

The detailed analysis is provided in Fig. 4(b) where the statistical results of deformation success rate as a function of release energy for different aging times were determined from Fig. 4(a). It is thus clear that the deformation success rate increases as the release energy increases at a given aging time. When the released

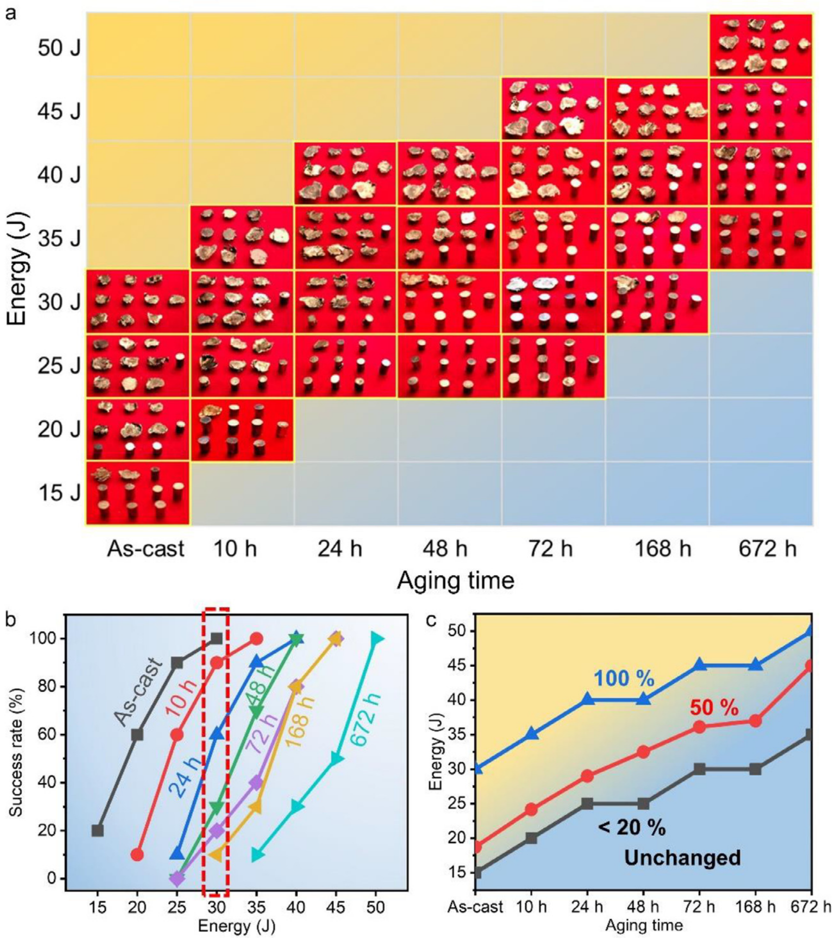

Fig. 4. Statistics of the softening of MGs by UV loading. (a) Photographs of samples obtained at different release energy values and aging times. Ten MG samples for each aging time and ultrasonic energy are shown. (b) Deformation success rate of MGs with different aging times as a function of UV loading energies. (c) Required ultrasonic energy as a function of aging time at different success rates. The curves represent the success rate below 20% (black curve), those around 50% (red curve), and 100% (blue curve).

energy is fixed, the deformation success rate decreases with increasing the aging time, as illustrated by the red dashed rectangle in Fig. 4(b). The deformation behaviors corresponding to the points in the red dashed rectangle are shown in Fig. S1 in the supplementary materials. The deformation success rate is determined accordingly.

In order to figure out the energy threshold change with the aging time, the energy value for a fixed deformation success rate is summarized in Fig. 4(c). Here we define the success rate below 20% as an unchanged region. It is clear that the required release energy increases as the aging time increases for all three cases with the success rate below 20%, around 50%, and 100%. As a result, the energy threshold required for deformation monotonously increases with extending the aging time.

3.3. Rejuvenation of aged samples after UV loading

It is clear that the long-term aged MGs can still be deformed by the UV loading, denoting that the processing and deformability of long-term aged MGs is no longer a technical problem in principle. We then tried to figure out the mechanism underlying this finding. Fig. 5(a) shows the enthalpy of the structural relaxation for the aged samples before and after the UV loading treatment. The blue dash line is the same as the enthalpy of the structural relaxation in Fig. 1(b), which gradually declines to zero as the aging time increases. The orange dash line exhibits the enthalpy of the structural relaxation of the samples after UV loading, which corresponds to the cyan area in Fig. 5(b). As shown in Fig. 5(a), after UV loading, the enthalpy of structural relaxation strongly increases. Quite intriguingly, the enthalpy value after UV loading is close to that of the as-cast sample and seems to be independent of the aging time. This result can also be confirmed by the DSC curves in Fig. 5(b), where the specific heat exotherms at different conditions almost completely overlap with each other. The inset of Fig. 5(b) exhibits the DSC curves of the samples with aging at 0.85T_g for 672 h before and after UV loading. It is noted that the enthalpy of structural relaxation is enhanced, while the enthalpy of the sub-T_g peak lowers after UV loading. As a result, UV loading strongly rejuvenates the aged sample and recovers the energy of the aged sample to the level of as-cast ones irrespective of the aging time.

The microstructure of the aged sample before and after UV loading is shown in Fig. 6. According to the HR-TEM images in Fig. 6(a) and XRD patterns in Fig. 6(b), all samples remain amorphous from the average structure down to the atomic level. Fig. 6(c) shows the electron diffraction intensity of the halo rings in the SAED patterns of four samples under different conditions, including an as-cast sample, 168-h aged one, 72-h aged one with UV loading, and 168-h aged one with UV loading. It is noted that the radius of the halo ring increases with aging but decreases after UV loading. The radius of the halo ring after UV loading is almost equivalent to that of the as-cast sample. The average atomic spacing is shown in Fig. 6(d), which is inversely proportional to the radius of the halo ring. It is clear that the average atomic spacing of the aged sample becomes lower than that of the as-cast one,

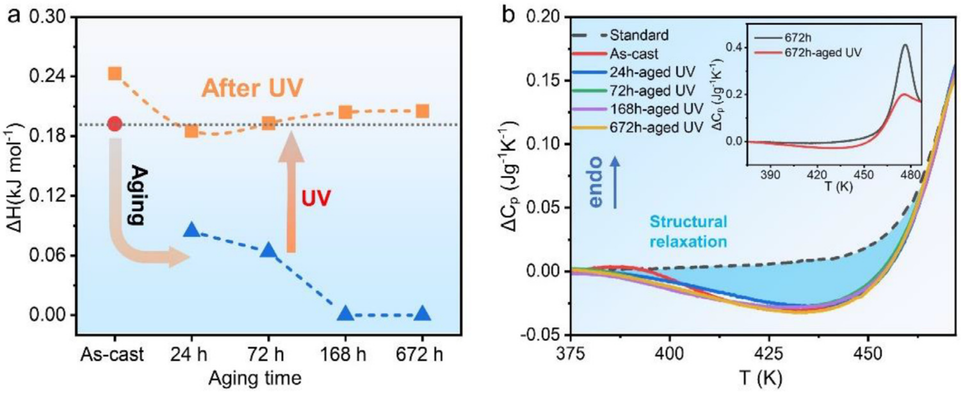

Fig. 5. Enthalpy change of aged samples before and after UV loading. (a) Enthalpy of structural relaxation process of aged samples before and after UV loading. The red dot represents the enthalpy of the as-cast sample, the blue curve shows the enthalpy after aging, and the orange line indicates the enthalpy after UV loading. (b) DSC curves of samples with different aging time after UV loading. The black dot curve is the same as the black curve in the inset of Fig. 1(b) and also serves as a standard curve here. The cyan area enclosed by the two curves corresponds to the enthalpy of the structural relaxation process. The black curve in the inset is the DSC curve aging at $0.85T_g$ for 672 h before UV loading. The red curve shows the DSC curve after UV loading.

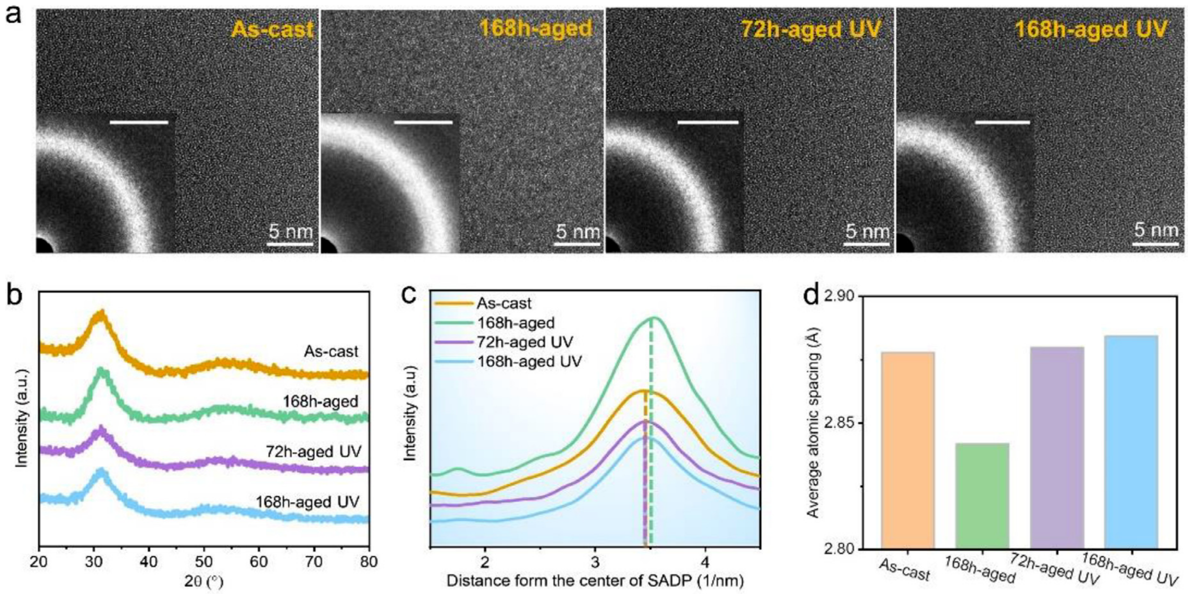

Fig. 6. Structure Characterization of samples before and after ultrasonic vibrational loading. (a) HR-TEM figures and SAED patterns of samples undergoing different treatments (As-cast sample, 168h-aged one, 72h-aged sample after UV loading (72h-aged UV), 168h-aged sample after UV loading (168h-aged UV)). The illustration has a scale of 2 1/nm. (b) XRD patterns after UV loading. (c) Diffraction ring radius obtained by SAED in (a). (d) Average atomic spacing obtained by diffraction ring radius.

which means that the amorphous structure becomes more densely packed after aging. Intriguingly, the average atomic spacing of the aged sample after UV loading is higher than that of the aged one before UV loading and is quite close to that of the as-cast one. This result indicates that the amorphous structure reverts to a loosely packed state after UV loading, similar to the state of the as-cast MGs. This is a rejuvenation process, and similar change made by other rejuvenation methods like cyclic loading has also been reported [44,60]. As a result, from the perspective of atomic structure, UV loading enables the aged MGs to rejuvenate, and the rejuvenated state is similar to the as-cast one.

3.4. Understanding the rejuvenation of aged glass by UV loading

Figs. 5 and 6 show that a rejuvenation process takes place accompanying the impressive UVIP. We then tried to explain the rejuvenation and deformation caused by UV loading according to a schematic microstructure and energy landscape. Fig. 7(a–c) exhibits the exothermic relaxation enthalpy changes after aging and UV loading. The broad exothermic peak disappears after aging in Fig. 7(b) and reappears after UV loading in Fig. 7(c). According to the literature [51], there are reversible and irreversible β-relaxations in as-cast MGs, which are illustrated by red atoms and cyan atoms respectively in Fig. 7(d). With increasing aging time, the cyan and red atoms gradually transform into blue atoms. Consequently, the cyan regions fully become blue finally, and the red regions also largely shrink in Fig. 7(e). As a result, the exothermic peak disappears and a sub-T_g peak overshoot occurs, as shown in Fig. 7(b). After UV loading, the structure becomes loosely packed again, so the red atoms increase and the cyan atoms reappear in Fig. 7(f), which corresponds to the reappearance of the exothermic peak at sub-T_g in Fig. 7(c).

To explain the rejuvenation of the aged sample under UV loading, we established a potential energy landscape (PEL) in Fig. 7(g), in which several potential energy minima/megabasins between different configurations are illustrated. The deepest energy minima on the PEL correspond to the stable crystalline phases, and other energy minima represent some metastable glassy states [2,57,61,62]. As-cast MGs are formed by the rapid cooling of the melt, and these deep and narrow pits are easily bypassed during the fast-cooling

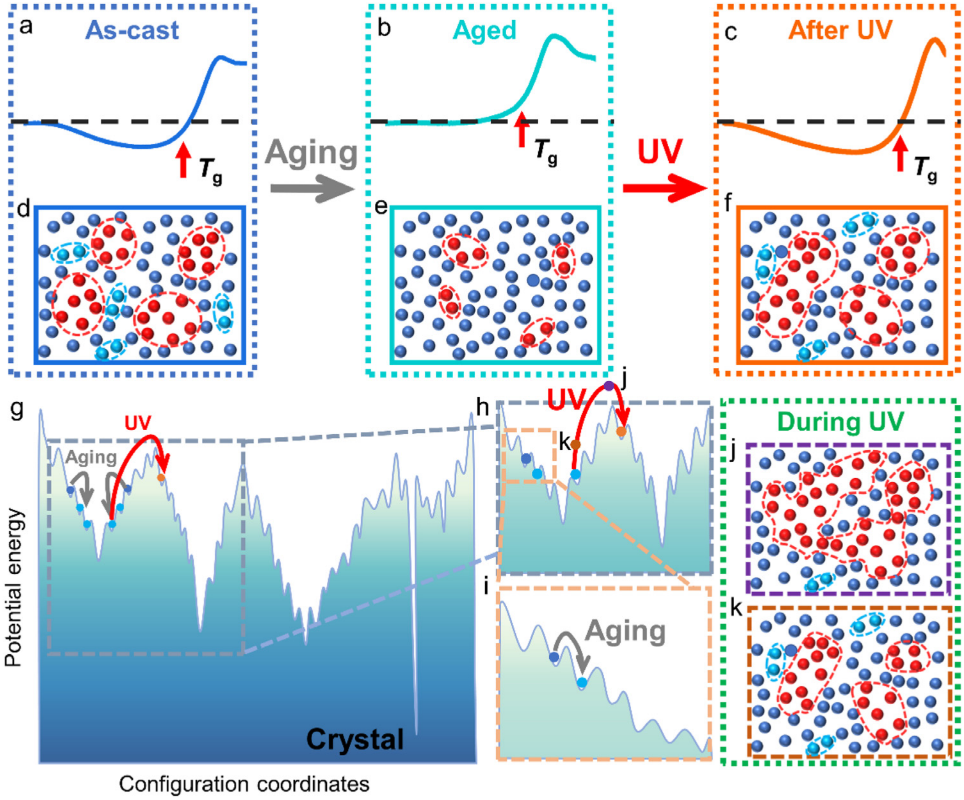

Fig. 7. Interpretation of the aging process and UV-induced rejuvenation of metallic glass. (a–c) DSC curves of metallic glass. (d–f) Schematic microstructures corresponding to DSC curves in (a–c). The red and cyan atomic regions represent areas contributing to reversible and irreversible β-relaxations in metallic glass, respectively. (g) Schematic diagram of the PEL of MGs. The dark blue ball denotes the energy state of as-cast metallic glass, the cyan ball stands for the energy state of metallic glass after aging, and the orange ball represents the energy state of metallic glass after UV loading. (h) The change in the energy state of aged metallic glass during UV loading (red arrow). (i) The change in the energy state of metallic glass during aging (gray arrows). (j–k) Schematic microstructure pictures during UV loading. (k) The atomic state corresponding to the activation of β-relaxation at the beginning of UV loading. (j) The atomic state corresponding to the fluid-like softening behavior during UV loading.

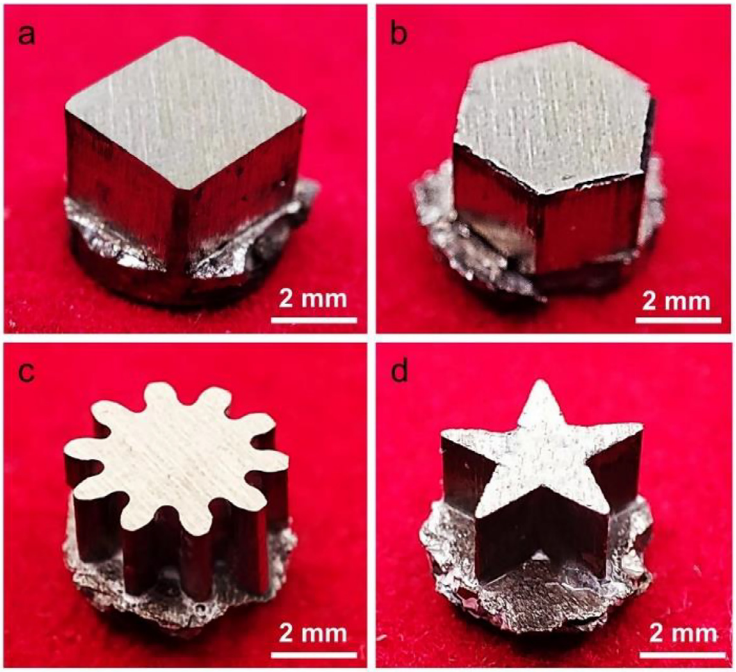

Fig. 8. Various shapes composed of aged metallic glass obtained by UV loading. The shapes include (a) rectangular prism, (b) hexagonal prism, (c) gear, and (d) pentagonal prism.

process of the melt. During the aging process, the as-cast samples tend to move to a more stable state, as shown in Fig. 7(i). When the aging time is long enough, the energy state of the aged MG becomes relatively low, so the exothermic peak disappears, as shown in Fig. 7(b). Once the aged samples undergo the UV loading treatment, the atomic regions corresponding to both the irreversible and reversible β-relaxations are excited, as illustrated in Fig. 7(k). Consequently, the state of the aged samples is injected to a higher energy level under UV loading in Fig. 7(h) and thus may trigger α-relaxations and cause a fluid-like softening behavior, as illustrated in Fig. 7(j). After UV loading, the MGs are located at an energy level similar to that of the as-cast MGs, so the connected red region in Fig. 7(j) transforms into localized red and cyan regions in Fig. 7(f).

Based on the above discussion, it is clear that UV loading enables the processing and molding of the aged MGs and makes them rejuvenate simultaneously, which is very suitable for shaping the aged MGs. We then tried to mold some shapes of the aged MGs through UV loading. The MGs aged at $0.85T_g$ for 48 h were used. As shown in Fig. 8, a variety of shapes are molded, including complex structures like gear (Fig. 8(c)) and pentagonal prism (Fig. 8(d)). Moreover, the whole process is carried out at room temperature through very low stress within a short time scale of 1 s. Therefore, we confirm that UV loading is a simple, feasible, and cost-effective solution for processing long-term aged metallic glass.

4. Conclusions

In summary, we have found that the aged MGs still exhibit excellent UVIP, even though they may achieve a relatively stable state with long-term aging. The UV energy threshold required to deform the aged sample monotonously increases with aging time. A strong rejuvenation is found accompanying the UVIP, and the relaxation enthalpy recovers to a level comparable to that of as-cast samples. This strong rejuvenation is explained through schematic microstructure pictures together with a schematic energy landscape. Complex-shaped structures are formed by using aged MGs under UV loading. This work indicates that UV-loading is a convenient and effective technique to deform and rejuvenate the aged MGs simultaneously, and thus may be a promising method to extend the application prospects of MGs.

Declaration of Competing Interest

The authors declare that they have no known competing financial interests or personal relationships that could have appeared to influence the work reported in this paper.

CRediT authorship contribution statement

Zhe Chen: Resources, Writing – review & editing. **Shuai Ren:** Conceptualization, Resources, Writing – review & editing. **Rui Zhao:** Writing – review & editing. **Jian Zhu:** Resources. **Xin Li:** Writing – review & editing. **Heting Zhang:** Resources. **Hongji Lin:** Resources. **Sajad Sohrabi:** Writing – review & editing. **Wenqing Ruan:** Resources. **Jiang Ma:** Conceptualization, Resources, Writing – review & editing.

Data availability

Data are available from the corresponding authors upon reasonable request.

Acknowledgments

The work was financially supported by the Key Basic and Applied Research Program of Guangdong Province, China (Grant No. 2019B030302010), the NSF of China (Grant Nos. 52122105, 51971150, and 51901243), the Science and Technology Innovation Commission Shenzhen (Grants No. RCJC20221008092730037 and 20220804091920001) and the National Key Research and Development Program of China (Grant No. 2018YFA0703605). The authors also thank the assistance on microscope observation received from the Electron Microscope Center of Shenzhen University.

Supplementary materials

Supplementary material associated with this article can be found, in the online version, at doi:10.1016/j.jmst.2023.09.029.

References

[1] M.D. Ediger, C.A. Angell, S.R. Nagel, J. Phys. Chem. 100 (1996) 13200–13212.
[2] P.G. Debenedetti, F.H. Stillinger, Nature 410 (2001) 259–267.
[3] A.L. Greer, Mater. Today 12 (2009) 14–22.
[4] L. Berthier, G. Biroli, Rev. Mod. Phys. 83 (2011) 587–645.
[5] M. Chen, NPG Asia Mater. 3 (2011) 82–90.
[6] D.C. Hofmann, J.Y. Suh, A. Wiest, G. Duan, M.L. Lind, M.D. Demetriou, W.L. Johnson, Nature 451 (2008) 1085–1089.
[7] W.H. Wang, Adv. Mater. 21 (2009) 4524–4544.
[8] D. Jang, J.R. Greer, Nat. Mater. 9 (2010) 215–219.
[9] M.X. Li, S.F. Zhao, Z. Lu, A. Hirata, P. Wen, H.Y. Bai, M. Chen, J. Schroers, Y. Liu, W.H. Wang, Nature 569 (2019) 99–103.
[10] L. Tian, Y.Q. Cheng, Z.W. Shan, J. Li, C.C. Wang, X.D. Han, J. Sun, E. Ma, Nat. Commun. 3 (2012) 609.
[11] C. Zhang, Z.X. Feng, Y.H. Zhang, Z.Z. Xia, N. Hakimi, T.M. Li, B.S. Xue, J. Tan, Vacuum 214 (2023) 112141.
[12] J. Schroers, Acta Mater. 56 (2008) 471–478.
[13] J. Schroers, Adv. Mater. 22 (2010) 1566–1597.
[14] J. Schroers, T. Nguyen, S. O'Keeffe, A. Desai, Mater. Sci. Eng. A 449 (2007) 898–902.
[15] G. Kumar, H.X. Tang, J. Schroers, Nature 457 (2009) 868–872.
[16] H.Z. Li, Z. Li, J. Yang, H.B. Ke, B.A. Sun, C.C. Yuan, J. Ma, J. Shen, W.H. Wang, Sci. China Mater. 64 (2021) 964–972.
[17] N. Li, X.N. Xu, Z.Z. Zheng, L. Liu, Acta Mater. 65 (2014) 400–411.
[18] K.-W. Park, C.-M. Lee, M. Wakeda, Y. Shibutani, M.L. Falk, J.-C. Lee, Acta Mater. 56 (2008) 5440–5450.
[19] S.C. Lee, C.M. Lee, J.C. Lee, H.J. Kim, Y. Shibutani, E. Fleury, M.L. Falk, Appl. Phys. Lett. 92 (2008) 151906.
[20] S.V. Ketov, Y.H. Sun, S. Nachum, Z. Lu, A. Checchi, A.R. Beraldin, H.Y. Bai, W.H. Wang, D.V. Louzguine-Luzgin, M.A. Carpenter, A.L. Greer, Nature 524 (2015) 200–203.
[21] Z. Peng, Y.M. Chen, G. Yin, P. Gong, Z. Jamili-Shirvan, N. Li, X.Y. Wang, K.F. Yao, Fundam. Res. 2 (2022) 764–775.
[22] Y. Tong, W. Dmowski, H. Bei, Y. Yokoyama, T. Egami, Acta Mater. 148 (2018) 384–390.
[23] D.V. Louzguine-Luzgin, V.Y. Zadorozhnyy, S.V. Ketov, Z. Wang, A.A. Tsarkov, A.L. Greer, Acta Mater. 129 (2017) 343–351.
[24] J. Pan, Y.P. Ivanov, W.H. Zhou, Y. Li, A.L. Greer, Nature 578 (2020) 559–562.
[25] K.M. Flores, E. Sherer, A. Bharathula, H. Chen, Y.C. Jean, Acta Mater. 55 (2007) 3403–3411.
[26] O. Haruyama, K. Kisara, A. Yamashita, K. Kogure, Y. Yokoyama, K. Sugiyama, Acta Mater. 61 (2013) 3224–3232.
[27] M. Stolpe, J.J. Kruzic, R. Busch, Acta Mater. 64 (2014) 231–240.
[28] J.W. Liu, Q.P. Cao, L.Y. Chen, X.D. Wang, J.Z. Jiang, Acta Mater. 58 (2010) 4827–4840.
[29] F.Q. Meng, K. Tsuchiya, S. Ii, Y. Yokoyama, Appl. Phys. Lett. 101 (2012) 121914.
[30] S.-H. Joo, D.-H. Pi, A.D.H. Setyawan, H. Kato, M. Janecek, Y.C. Kim, S. Lee, H.S. Kim, Sci. Rep. 5 (2015) 9660.
[31] W. Dmowski, Y. Yokoyama, A. Chuang, Y. Ren, M. Umemoto, K. Tsuchiya, A. Inoue, T. Egami, Acta Mater. 58 (2010) 429–438.
[32] C. Ebner, B. Escher, C. Gammer, J. Eckert, S. Pauly, C. Rentenberger, Acta Mater. 160 (2018) 147–157.
[33] Y.H. Sun, A. Concustell, A.L. Greer, Nat. Rev. Mater. 1 (2016) 16039.
[34] X. Li, J.G. Wang, H.B. Ke, C. Yang, W.H. Wang, Mater. Today Phys. 27 (2022) 100782.
[35] X.N. Yang, H. Tong, W.H. Wang, K. Chen, J. Stat Mech-Theory Exp. 2020 (2020) 024007.
[36] M. Zhang, Y.M. Wang, F.X. Li, S.Q. Jiang, M.Z. Li, L. Liu, Sci. Rep. 7 (2017) 625.
[37] D. Bonn, S. Tanase, B. Abou, H. Tanaka, J. Meunier, Phys. Rev. Lett. 89 (2002) 015701.
[38] V. Viasnoff, F. Lequeux, Phys. Rev. Lett. 89 (2002) 065701.
[39] J. Pan, Y.X. Wang, Q. Guo, D. Zhang, A.L. Greer, Y. Li, Nat. Commun. 9 (2018) 560.
[40] I.M. Hodge, Science 267 (1995) 1945–1947.
[41] R. Casalini, C.M. Roland, Phys. Rev. Lett. 102 (2009) 035701.
[42] B. Ruta, E. Pineda, Z. Evenson, J. Phys. Condens. Matter. 29 (2017) 503002.
[43] J. Ma, C. Yang, X.D. Liu, B.S. Shang, Q.F. He, F.C. Li, T.Y. Wang, D. Wei, X. Liang, X.Y. Wu, Y.J. Wang, F. Gong, P.F. Guan, W.H. Wang, Y. Yang, Sci. Adv. 5 (2019) eaax7256.

[44] X. Li, D. Wei, J.Y. Zhang, X.D. Liu, Z. Li, T.Y. Wang, Q.F. He, Y.J. Wang, J. Ma, W.H. Wang, Y. Yang, Appl. Mater. Today 21 (2020) 100866.

[45] Z. Huang, J. Fu, X. Li, W. Wen, H. Lin, Y. Lou, F. Luo, Z. Zhang, X. Liang, J. Ma, Sci. China Mater. 65 (2021) 255–262.

[46] W.H. Wang, Prog. Mater. Sci. 106 (2019) 100561.

[47] H.-B. Yu, W.-H. Wang, K. Samwer, Mater. Today 16 (2013) 183–191.

[48] P. Luo, Z. Lu, Z.G. Zhu, Y.Z. Li, H.Y. Bai, W.H. Wang, Appl. Phys. Lett. 106 (2015) 031907.

[49] H.B. Yu, W.H. Wang, H.Y. Bai, K. Samwer, Nat. Sci. Rev. 1 (2014) 429–461.

[50] J.D. Stevenson, P.G. Wolynes, Nat. Phys. 6 (2009) 62–68.

[51] R. Zhao, H.Y. Jiang, P. Luo, L.Q. Shen, P. Wen, Y.H. Sun, H.Y. Bai, W.H. Wang, Phys. Rev. B 101 (2020) 094203.

[52] A. van den Beukel, J. Sietsma, Acta Metall. Mater. 38 (1990) 383–389.

[53] P. Luo, Z. Lu, Y.Z. Li, H.Y. Bai, P. Wen, W.H. Wang, Phys. Rev. B 93 (2016) 104204.

[54] Y. Yue, C.A. Angell, Nature 427 (2004) 717–720.

[55] A.Q. Tool, J. Am. Ceram. Soc. 29 (1946) 240–253.

[56] P. Badrinarayanan, W. Zheng, Q.X. Li, S.L. Simon, J. Non-Cryst. Solids 353 (2007) 2603–2612.

[57] Y. Zhao, B. Shang, B. Zhang, X. Tong, H. Ke, H. Bai, W.H. Wang, Sci. Adv. 8 (2022) eabn3623.

[58] H.B. Yu, X. Shen, Z. Wang, L. Gu, W.H. Wang, H.Y. Bai, Phys. Rev. Lett. 108 (2012) 015504.

[59] S. Vyazovkin, I. Dranca, Pharm. Res. 23 (2006) 422–428.

[60] G. Ding, C. Li, A. Zaccone, W.H. Wang, H.C. Lei, F. Jiang, Z. Ling, M.Q. Jiang, Sci. Adv. 5 (2019) eaaw6249.

[61] C. Pei, S. Chen, T. Zhao, M. Li, Z. Cui, B. Sun, S. Hu, S. Lan, H. Hahn, T. Feng, Adv. Mater. 34 (2022) e2200850.

[62] J. Jiang, Z. Lu, J. Shen, T. Wada, H. Kato, M. Chen, Nat. Commun. 12 (2021) 3843.